Visions and Strategies for Reinforcing Additively Manufactured Constructions 2025

Contribution to the symposium

https://doi.org/10.52825/ocp.v7i.2776



Published: 12 Dec. 2025

# Integrated Fiber Forms – Functionally Integrated Slab Systems through Additive Manufacturing and Natural Fiber Reinforcement

Conference Paper

Bruno Knychalla[1,*], Christian Wiesner[1], Patrick Sonnleitner[1], Magdalena Kowalczyk[2], Allin Groom[2], and Peter Storey[3]

[1]additive tectonics GmbH, DE

[2]Autodesk Research, Autodesk Ltd, UK

[3]Autodesk Research, Autodesk B.V., NL

*Correspondence: Bruno Knychalla, bruno.knychalla@additive-tectonics.com

**Abstract:** Today's structural floor systems are labour-intensive to install and constrained to orthogonal shapes, relying on formwork that leads to material waste and elevated carbon emissions. This research introduces a particle-bed 3D-printed, stay-in-place formwork produced from upcycled wood-aggregate. The formwork defines the geometry of the slab, enabling complexity and performance-optimization. Instead of conventional steel reinforcement, robotically wound flax fiber cords are anchored to winding points integrated directly into the printed formwork. Combined with cast geopolymer, this approach eliminates the risk of corrosion and significantly reduces embodied carbon. Because the formwork remains in place, no dismantling or disposal is required, resulting in substantial reductions in labour and construction waste. The system's topology-optimised geometry improves ceiling-specific acoustic performance, accommodates embedded utility conduits, and can reduce the need for suspended ceil-ings and thus maximise usable space. The result is a lightweight, trade-friendly floor system that points towards functional and environmental advantages. Its feasibility has been demonstrated at architectural scale through a 1:1, four meter, prototype.

**Keywords:** Particle-Bed AM, 3D Printing, Concrete Printing, Selective Cement Activation, Fibre Winding, Formwork, Geopolymer, Hybrid Construction

## 1. Introduction

Structural floor systems remain among the most labour- and material-intensive building elements. Conventional slabs rely on temporary formwork, and contribute significantly to the building industry's waste and carbon emissions problem. Particle-bed additive manufacturing (PBAM) offers an alternative: prefabrication without standard-ized formwork and with geometric freedom to combine structural performance, acoustic behaviour, and service integration.

This study investigates a manufacturing route for a hybrid ceiling element in which a PBAM wood-magnesia shell remains in place, prefiguring winding nodes for continuous, stress-aligned flax reinforcement, followed by casting of a geopolymer compression layer. The contribution lies in coupling stay-in-place, high-resolution PBAM formwork with on-part, stress-aligned tensile reinforcement at architectural scale. The presented paper concentrates on full-scale process description and feasibility (geometry derivation, printing, winding path generation and execution, and casting) while deferring systematic structural evaluation, in-depth material investigations, and environmental comparison to future work.

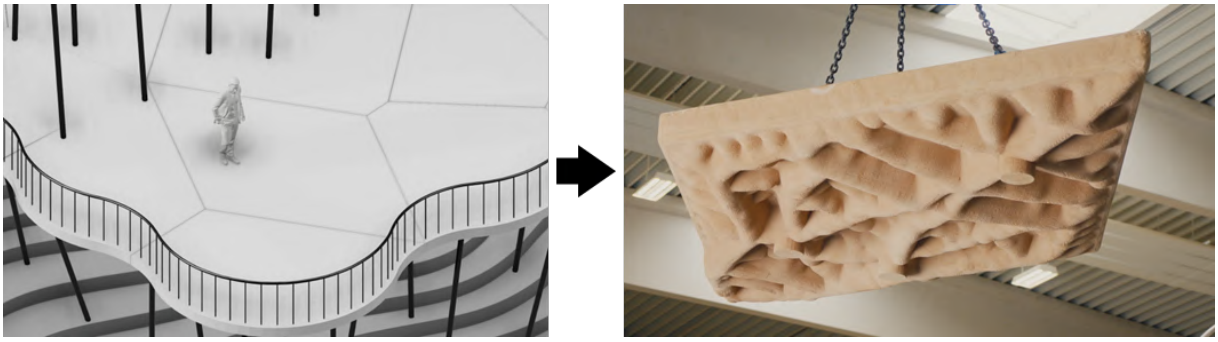

***Figure 1.*** *Illustration of the 1:1 prototype in architectural context. Left: proposed architectural design showing the diamond floor slab in situ. Right: completed full-scale prototype. The arrow indicates the translation from design intent to manufactured element.*

## 2. State of the Art

A large share of a building's mass and embodied carbon resides in the floor–ceiling system [1]. Conventional cast-in-place and precast slabs are governed by formwork logistics and straight-bar reinforcement; they tend to be single-function elements of uniform thickness, even where load paths and service routing would justify more differentiated geometries [2]. Building services are typically accommodated in suspended ceilings, increasing overall depth and material use. These constraints motivate fabrication approaches that deliver assembly-grade accuracy with construction-grade materials, enabling structurally efficient, functionally integrated ceiling systems [3].

Particle-bed additive manufacturing (PBAM) with construction materials has progressed from academic demonstrators [4] to industrial prefabrication for large components [5]. In Selective Cement Activation (SCA), a subtype of PBAM, the compacted particle bed consists of construction aggregates with a latent (dry) mineral binder onto which a liquid activator is selectively jetted to trigger local setting and bind successive layers [6]. Working directly with construction materials enables ribbing, voiding, and integrated conduits in as-printed parts [7], suitable for horizontal building elements that are made without conventional formwork [8].

Within this landscape, ETHZ Digital Building Technologies has demonstrated 3D-printed formwork for slab systems which included stay-in-place solutions [9] and post-tensioned assemblies [10] where the printed components primarily provide geometry and casting control. Although using high-resolution PBAM, these projects do not implement continuous stress-aligned tensile reinforcement. Similarly, ILEK (University of Stuttgart) has produced PBAM formwork for complex stress-aligned horizontal concrete structures using particle-bed approaches that integrate fibers [11]. Here, the emphasis lies on water-soluble formwork and temporary placement of prefabricated fibrous reinforcement rather than integrating a PBAM part into the ceiling. Both ap-

proaches demonstrate the geometric potential of PBAM for building slabs, however neither uses PBAM as an enabler for stress-aligned tensile reinforcement. Recently, there has been increasing development in robotic fiber winding as a strategy to produce architectural parts with continuous stress-aligned tensile reinforcement [12]. At the University of Stuttgart, IntCDC, architectural demonstrators were produced through natural fiber (flax) winding where the wound system is the structure itself [13]; these works are additive manufacturing by nature, but they do not serve as tensile reinforcement within a multi-functional closed ceiling system. In parallel, TU Braunschweig combines robotic winding with shotcrete/extrusion-based printing [14] to embed continuous fibers in concrete elements. However, the winding is not performed on high-resolution PBAM parts. Furthermore, the target typologies are not ceiling slabs, and fibers are wound onto frames or onto freshly printed shotcrete and then over-sprayed without the 3D Printing enabling the fiber reinforcement.

To conclude, prior work either uses PBAM to shape formwork geometry without on-part, stress-aligned continuous reinforcement, or it uses robotic winding with extrusion/shotcrete rather than PBAM, and not for ceiling slabs. This paper introduces a novel method of fabricating a full-scale PBAM ceiling in which a stay-in-place mineral part both pre-forms the slab geometry and enables stress-aligned reinforcement. Here, we present such a system in combination with robotically wound continuous flax fiber reinforcement and cast geopolymer.

## 3. Method

### 3.1 Digital pipeline: analysis, trajectories, geometry

A slab model was prepared in Autodesk Inventor and analysed under representative service loading conditions, accounting for both live loads and self-weight, and supported in line with conventional boundary configurations. Topology optimisation (Inventor Nastran) was set up to achieve a substantial mass reduction while limiting the allowable global stiffness loss; resolution constraints were enforced through a minimum feature size parameter. Principal tensile stresses from linear static analysis were normalised to $\sigma/\sigma_{\text{max}}$ and converted into a medial-axis network. Fiber winding density was then modulated by the stress field, ensuring that regions experiencing higher tension received proportionally more reinforcement passes (see Section 3.3).

The stress bitmap was imported to Rhinoceros/Grasshopper, sampled on a 10 mm grid, and mapped to shell thickness using

$$t(x, y) = t_{\min} + (t_{\max} - t_{\min}) \cdot \frac{\sigma}{\sigma_{\max}},$$

with $t_{\min} = 12$ mm and $t_{\max} = 50$ mm.

Principal tensile stress vectors defined a spatial winding demand. Winding nodes were placed at vector–field junctions with a prong count $\geq 3$ (i.e., multiple incoming principal directions). Additional nodes were inserted manually in high-curvature regions to prevent fiber–formwork contact. Winding nodes were modelled as printed bosses with filleted grooves sized to accommodate up to 26 winds of the 3 mm roving. The output geometry was exported as a watertight STL for printing and as a point cloud (CSV) for robotic path planning (see Figure 2).

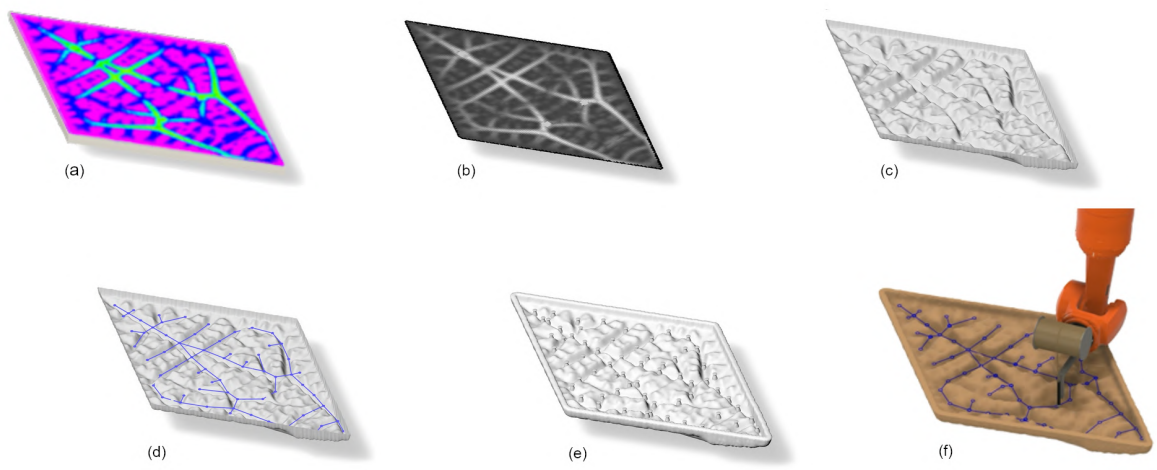


***Figure 2.*** *Digital pipeline: (a) loading conditions defined and analysed in Inventor Nastran; (b) greyscale stress bitmap generated; (c) bitmap mapped to produce the formwork shell; (d) principal tensile vectors extracted and toolpath strategy defined; (e) fiber winding nodes established at vector intervals and junctions; (f) toolpath simulation conducted to resolve clearance issues during fabrication.*

### 3.2 PBAM stay-in-place formwork

The large-scale formwork ($3650 \times 2128 \times 297$ mm$^3$; $160$ dm$^3$ total volume) was fabricated using a gantry-based SCA system, providing a build volume of $2.3 \times 3.8 \times 0.9$ m$^3$ (Figure 4) .
Printing was performed in 198 1.5 mm layers, resulting in a predicted total build time of $\sim$2.5 h.
The feedstock comprised untreated beechwood particles ($\leq 2mm$), caustic magnesium oxide and additives.
Aqueous activator fluid is deposited through a 2,500-nozzle printhead, inducing gel-formation and solidification at the liquid–powder interfaces, providing sufficient strength for unpacking after about 12 hours.
Process monitoring included co-printed prisms (40 × 40 × 160 mm$^3$) and a cylinder for thermal measurements.
Three prisms each were tested in accordance with DIN EN 196-1 for compressive and bending strength after 5, 10, and 30 days. Dimensional accuracy and part density was also obtained from those specimens.
Thermocouples inside the cylinder recorded reaction temperature.
After unpacking, the part's surface was vacuum-cleaned and coated with a water-based acrylate primer ($180 \pm 10$ g/m$^2$) and cured at $23 \pm 2$ ℃ and $50 \pm 5$% RH for 24 h.
The unreacted material (93% of the powder in the print envelope) was vacuumed, sieved and fully recirculated into the SCA process.

### 3.3 Fibre winding path generation and execution

Through the path model of Section 3.1, paths between nodes were assigned a local winding count proportional to the normalised stress, $\sigma/\sigma_{\text{max}}$, with a maximum of seven passes. Seven passes were found to provide the required strength for the maximum tensile stress expected in the element.

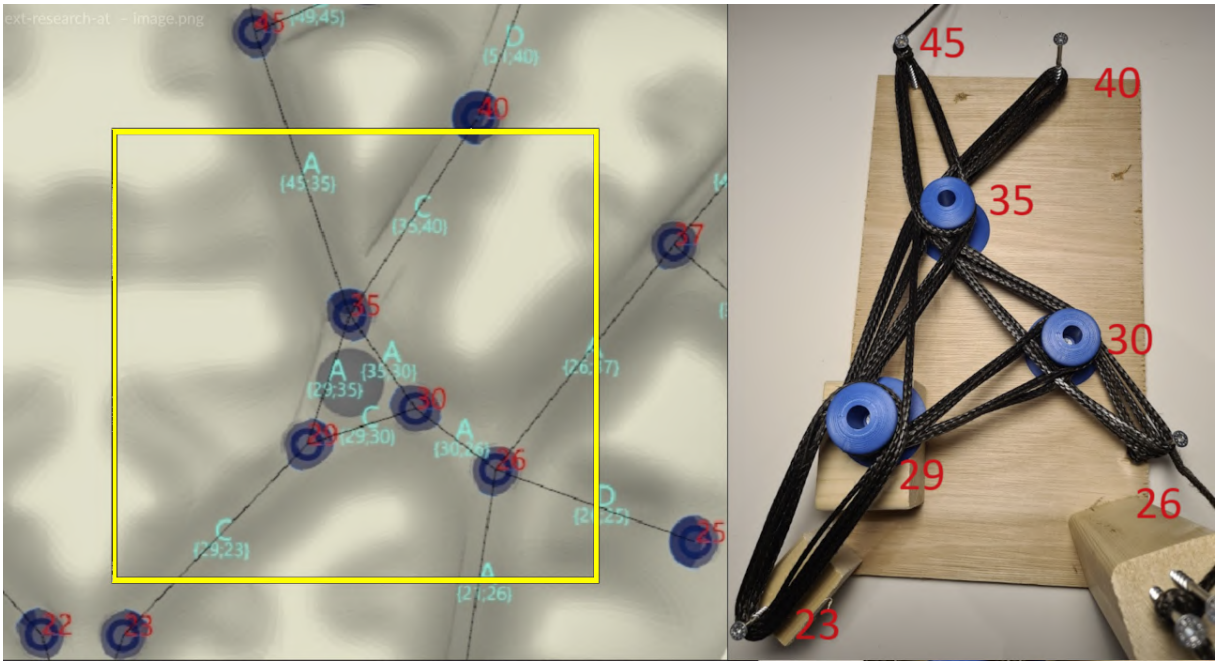


***Figure 3.*** *Left: Digital model of the most congested part of the formwork. Numbered nodes sit at different heights, a layout that can cause fibre slippage during winding. Right: The same junction in the prototype. It sits in the highest-tension zone and carries the greatest number of fibre winds; manual winding here proved feasible for robot automation.*

In Autodesk Dynamo, this node-edge set was converted into a weighted multigraph, where each edge weight corresponded to its required number of passes. A route-inspection algorithm (Guan's Route Problem [15], [16]) was applied to produce a single continuous winding path that covers all required segments with minimal additional traversals.

The ordered XYZ coordinates were converted into KUKA KRL motion instructions for execution on a 6-axis KUKA KR210 on a 7th-axis rail (reach 3.2 m; repeatability ±0.06 mm). Three-millimetre flax cords were laid along this path. Winding tension was not instrumented; end-effector parameters were tuned empirically.

To reduce water uptake, fuse bundles, and enhance bond to the mineral matrix, the cords were post-impregnated *in situ* with a low-viscosity bisphenol-A/epichlorohydrin epoxy ($\eta_{2.5\,^\circ\mathrm{C}} = 400 \pm 20$ MPa·s) using a dot-dab brush technique to ensure full bundle wet-out prior to casting.

### 3.4 Geopolymer mortar, casting, and curing

The geopolymer cast contained 20 wt.% metakaolin Mk-750 (Imerys S.A., Paris), 25 wt.% aqueous potassium silicate solution (Wöllner GmbH, Ludwigshafen), 10 wt.% potassium feldspar (Gebrüder Dorfner GmbH & Co. KG, Hirschau), and 45 wt.% washed silica sand graded 0.1-5 mm (Wolff & Müller Quarzsande GmbH). The constituents were blended for 15 min in a 50 L counter-current pan mixer.
Approximately 580 litre ($\sim$1.20 t) of fresh geopolymer was cast into the formwork in four batches, slowly to fill rib and node features without entrapped air. The exposed surface was sealed with a 0.2 mm polyethylene sheet; curing proceeded at ambient conditions ($\approx$22 °C, 46 $\pm$ 4% RH) for 14 days. No thermal curing was applied.

***Figure 4.*** *Left: Particle-bed printing of the full-scale (4 m) formwork, completed in 2 h 29 min. Right: Loose powder is vacuumed away and recycled, exposing the finished part.*

# 4. Results

## 4.1 Simulation and Data Preparation

The ceiling element underwent coordinated architectural design, performance simulation, robotic fibre-winding simulation, and detailing. Rather than optimising for a single criterion, the design balanced multiple objectives. Interdependencies made early assumptions consequential; for example, the end-effector was not fully defined during initial winding simulation, which led to inaccurate clearance checks that were corrected later (see 4.3). Wall thickness was governed primarily by casting pressure constraints rather than acoustic or structural targets.

## 4.2 Printing and formwork behaviour

The full-scale formwork was printed successfully in 2 h 29 min. Thermocouples inside a designated cylinder recorded reaction temperature during curing, peaking at 69.8 °C at the 12 hour mark, defining the time for safe unpacking. The produced part, weighing 144 kg, was removed by crane while sitting on a 40 cm steel platform and a transportation frame. Dimensional verification showed an acceptable tolerance of +3 mm across the component. Mechanical testing (DIN EN 196-1) of the co-printed wood-composite specimens showed good early strength after 5 days and a typical development of flexural and compressive strength with sample age ( Figure 5 ) and provide a compressive strength of 5.6 to 9.0 MPa and a flexural strength of 3.2 to 4.7 MPa.

The measured values were within the expected range and allowed safe handling and cleaning of the large mould after five days. Thus, all requirements for the mould were met. However, the entire cast and reinforced element is designed to withstand loads significantly higher than those supported by the formwork itself. A reliable prediction of the load-bearing capacity requires detailed knowledge of the properties of these specific flax-fibres and the geopolymer matrix (e. g. Young's modulus, tensile strength, exact fibre cross-section, fibre–matrix adhesion). These datasets are currently being collected and will be evaluated in a separate publication

Density also showed normal values for this material system with no significant changes due to possible interactions with the ambience over time. The slight increase in sample weight per volume, visible at the 30 days mark, is attributed to very minor water uptake.

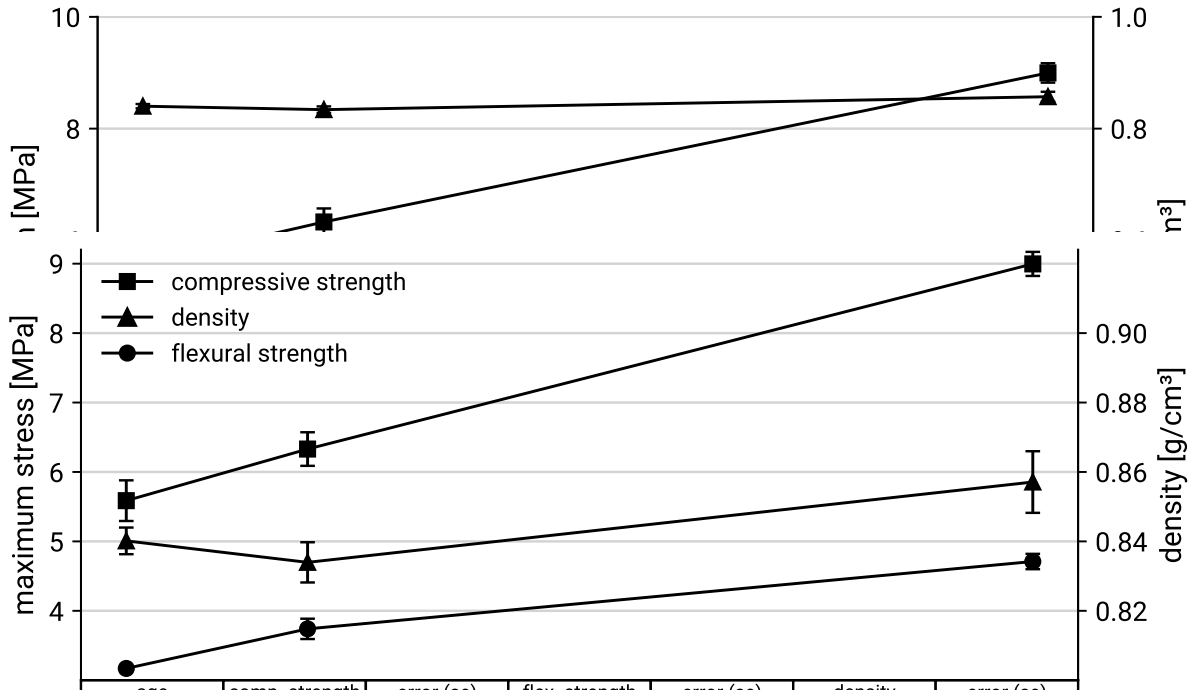


| age | comp. strength | error (se) | flex. strength | error (se) | density | error (se) |
|---|---|---|---|---|---|---|
| 5 | 5.59 | 0.293 | 3.17 | 0.032 | 0.84 | 0.004 |
| 10 | 6.33 | 0.242 | 3.74 | 0.146 | 0.83 | 0.006 |
| 30 | 9.00 | 0.173 | 4.71 | 0.111 | 0.86 | 0.009 |

***Figure 5.*** *Formwork Material: Development of mechanical properties over time. Data table shows average maximum stress in MPa and average density in g/cm³ for three specimen each, standard error*

The demonstrator was unpacked outside the machine with residual particles intentionally left beneath for support. Priming, winding, and casting were performed on this supported setup. Working around loose particles introduces practical risks (workspace safety, risk of particulate deposition on critical surfaces and fluids, local loss of support), which were managed during the prototype but should be addressed in future fixtures and procedures.

### 4.3 Winding performance and node behaviour

The stress-proportional winding density was achieved as designed, and the route-inspection toolpath enabled one continuous winding operation. Winding tension was not instrumented; end-effector settings were tuned empirically. During initial passes, several printed nodes split under local bearing; after through-thickness screw reinforcement of those nodes and adjustment of end-effector tension settings, winding proceeded without further node failure. Clearances in dense node fields were tight until the end-effector geometry was revised to reduce clashes (consistent with the simulation limitation noted in 4.1).

### 4.4 Casting and curing

Gravity placement filled ribs, cavities, and node regions satisfactorily.
After fourteen days of ambient curing, the slab retained its geometry without global warping and the geopolymer–to-formwork adhesion and mechanical interlock ap-


***Figure 6.*** *Fabrication sequence of the formwork: (a) after printing and loose powder is removed, a robot winds continuous flax fibres over the shell. The robot successfully negotiated congested node junctions without slippage or clearance issues (b); (c) once the fibres are epoxy-impregnated, a geopolymer is manually poured into the cavity; (d) the fluid mix flows readily through the formwork, leaving only negligible entrapped air.*

peared sound, even though minor local delamination on the geopolymer-formwork interface appeared.
The geopolymer surface presented a homogeneous appearance without chalking or friability. Net-shaped superficial cracking was visible on the exposed surface and is attributed to local evaporation where sealing was imperfect; no structural shrinkage cracking was observed.
Once reinforced, the demonstrator could be suspended and moved from above, indicating a marked improvement in handling stiffness and integrity.

## 5. Discussion

This exploration shows that PBAM/SCA can produce a stay-in-place, ceiling-optimized formwork at architectural scale with short print times and tight tolerances. Here, the PBAM-shell was not designed as an element that needs reinforcement, but as an enabler for winding fibres along principal stress lines.

In simulation, the end-effector was not yet fully defined, which limited early checks clearances, and the subsequent geometry change resolved clashes. Printed winding nodes enabled on-part winding but showed first-generation mechanics: local splitting under bearing required screw reinforcement. Going forward, tool-clearance and curvature rules should be encoded in the parametric model. Because winding tension was not measured, process repeatability and the relationship between fibre stress, node loading, and global behaviour remain unquantified.

The combination of barrier primer, epoxy-impregnated flax, and sealed ambient cure limited shrinkage effects to superficial surface cracking linked to imperfect sealing. Epoxy ensured process reliability but is environmentally burdensome [17]; a mineral or bio-based alternative (e.g., geopolymer-compatible sizing) should be investigated

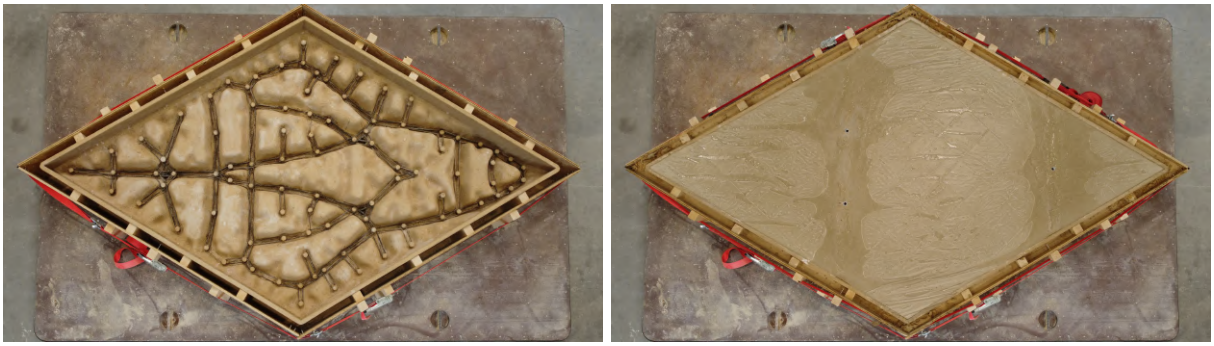

***Figure 7.*** *Left: Formwork after robotic fibre winding and epoxy impregnation, ready for casting. Right: Same element after geopolymer casting and curing; the shallow surface undulations are the imprint of the sealing membrane used to retain moisture and prevent shrinkage cracking.*

[18]. Certain steps (priming, winding, and casting) where executed when the part was semi-unpacked, which is feasible for low volume production, but constrains handling and introduces powder-related risks.

## 6. Conclusion and Outlook

A hybrid slab combining PBAM-printed, stay-in-place wood–magnesia formwork, robotically wound flax reinforcement, and a cast geopolymer compression layer was demonstrated at architectural scale. Printing achieved +3 mm accuracy in 2 h 29 min. Continuous winding on integrated nodes was achieved; early node fractures were retrofit-reinforced with screws, allowing completion. The topology-guided geometry integrates structural ribbing, texture, and service conduits, and points toward a trade-friendly and acoustically well performing system that eliminates demoulding and reduces waste. Fabrication gaps: (i) uninstrumented winding tension; (ii) node load-transfer capacity, especially for multiple winds; and (iii) replacement of epoxy with a lower-impact fiber matrix. The method is process-feasible at full scale and provides a practical route for additively manufactured, reinforced ceiling systems.

Future investigations should address, first, system-level mechanical behaviour at element scale to situate the typology within a design framework. Second, composite mechanics need clarification at the key interfaces of fiber–geopolymer, geopolymer–formwork, and the printed winding nodes; so that load transfer, anchorage, and failure modes are characterised. Third, a comparative assessment of environmental impact against conventional ceiling systems would indicate where material savings and trade integration yield meaningful reductions at building scale. Finally, the geometric and structural potential of more spatial, truss-like reinforcement winding for horizontal elements should be investigated for structural and architectural performance.

## Author contributions

Writing original draft: Bruno Knychalla
Writing review/editing: Allin Groom, Peter Storey, Patrick Sonnleitner, Bruno Knychalla
Software: Magdalena Kowalczyk, Peter Storey
Project supervision: Bruno Knychalla
Project administration: Peter Storey and Christian Wiesner

***Figure 8.*** *Completed 4 meter span prototype floor slab. The stay-in-place, 3D-printed formwork and the continuous flax-fibre winding now act as a single, integrated load-bearing system.*

## Competing interests

The authors declare no competing interests.

## Acknowledgements

The authors gratefully acknowledge the Autodesk Technology Centre in Boston for providing access to facilities, expert guidance, and hands-on assistance throughout the prototyping and testing stages of this research.

## References

[1] A. Jayasinghe, J. Orr, W. Hawkins, T. Ibell, and W. P. Boshoff, "Comparing different strategies of minimising embodied carbon in concrete floors," *Journal of Cleaner Production*, vol. 345, p. 131 177, 2022, ISSN: 0959-6526. DOI: https://doi.org/10.1016/j.jclepro.2022.131177. [Online]. Available: https://www.sciencedirect.com/science/article/pii/S0959652622008083.

[2] F. Ranaudo, T. Mele, and P. Block, "A low-carbon, funicular concrete floor system: Design and engineering of the hilo floors," Jan. 2021, pp. 2016–2024. DOI: 10.2749/ghent.2021.2016.

[3] A. Jipa, G. Lydon, A. Yoo, G. Chousou, B. Dillenburger, and A. Schlueter, "Hires: 3d-printed formwork for an integrated slab," in *Scalable Disruptors*, P. Eversmann, C. Gengnagel, J. Lienhard, M. Ramsgaard Thomsen, and J. Wurm, Eds., Cham: Springer Nature Switzerland, 2024, pp. 423–433, ISBN: 978-3-031-68275-9.

[4] D. Lowke, E. Dini, A. Perrot, D. Weger, C. Gehlen, and B. Dillenburger, "Particle-bed 3d printing in concrete construction ‚äì possibilities and challenges," *Cement and Concrete Research*, vol. 112, pp. 50–65, 2018, SI : Digital concrete 2018, ISSN: 0008-8846. DOI: https://doi.org/10.1016/j.cemconres.2018.05.018. [Online]. Available: https://www.sciencedirect.com/science/article/pii/S000888461731267X.

[5] S. Frank. "Digital materials for digital construction." Accessed: 2025-08-29. (2021), [Online]. Available: https://www.autodesk.com/de/design-make/articles/3d-printing-in-construction-industry.

[6] D. Talke, K. Henke, and D. Weger, "Selective cement activation (sca)–new possibilities for additive manufacturing in construction," in *Proceedings Of IASS annual symposia*, International Association for Shell and Spatial Structures (IASS), vol. 2019, 2019, pp. 1–8.

[7] J. Fleckenstein, D. Briels, A. Baghdadi, *et al.*, "Breuer x am: Functional hybridisation in concrete building envelope elements through additive manufacturing," in Apr. 2024, pp. 196–205, ISBN: 9781800086357. DOI: 10.2307/jj.11374766.29.

[8] S. Dietrich, P. Schneider, C. Richter, *et al.*, "Multi-fidelity structural design for 3d concrete printing with selective paste intrusion," *Automation in Construction*, vol. 179, p. 106 352, 2025.

[9] A. Jipa, M. Bernhard, M. Meibodi, and B. Dillenburger, "3d-printed stay-in-place formwork for topologically optimized concrete slabs," in *Proceedings of the 2016 TxA emerging design+ technology conference*, Texas Society of Architects, 2016, pp. 97–107.

[10] A. Anton and A. Pronk, "Optimised pattern for a beam under combined loading," Unpublished manuscript, 2017.

[11] P. Block, G. Boller, C. DeWolf, J. Pauli, and W. Kaufmann, "Structural design and analysis of marinaressa coral tree," 2024.

[12] M. Prado, M. Drstelmann, T. Schwinn, A. Menges, and J. Knippers, "Core-less filament winding," May 2014, ISBN: 978-3-319-04662-4. DOI: 10.1007/978-3-319-04663-1_19.

[13] P. Mindermann, M. Gil P©rez, J. Knippers, and G. T. Gresser, "Investigation of the fabrication suitability, structural performance, and sustainability of natural fibers in core-less filament winding," *Materials*, vol. 15, no. 9, 2022, ISSN: 1996-1944. DOI: 10.3390/ma15093260. [Online]. Available: https://www.mdpi.com/1996-1944/15/9/3260.

[14] S. Gantner, T.-N. Rothe, C. Hºhne, and N. Hack, "Reinforcement strategies for additive manufacturing in construction based on dynamic fibre winding: Concepts and initial case studies," *Open Conference Proceedings*, vol. 1, pp. 45–59, Feb. 2022. DOI: 10.52825/ocp.v1i.78. [Online]. Available: https://www.tib-op.org/ojs/index.php/ocp/article/view/78.

[15] M.-K. Kwan, "Graphic programming using odd or even points," *Chinese Mathematics*, vol. 1, pp. 273–277, 1962.

[16] H. A. Eiselt, M. Gendreau, and G. Laporte, "Arc routing problems, part II: The rural postman problem," *Operations Research*, vol. 43, no. 3, pp. 399–414, 1995. DOI: 10.1287/opre.43.3.399.

[17] A. La Rosa, G. Recca, J. Summerscales, A. Latteri, G. Cozzo, and G. Cicala, "Bio-based versus traditional polymer composites. a life cycle assessment perspective," *Journal of Cleaner Production*, vol. 74, Jul. 2014. DOI: 10.1016/j.jclepro.2014.03.017.

[18] J. A. Abdalla, R. A. Hawileh, A. Bahurudeen, *et al.*, "A comprehensive review on the use of natural fibers in cement/geopolymer concrete: A step towards sustainability," *Case Studies in Construction Materials*, vol. 19, e02244, 2023, ISSN: 2214-5095. DOI: https://doi.org/10.1016/j.cscm.2023.e02244. [Online]. Available: https://www.sciencedirect.com/science/article/pii/S2214509523004242.